6

Soft Lithography strategies for fabricating polymeric microtube for effective dye degradation

This chapter explores the fabrication of polymeric functional platforms decorated with ZnO-based nanocomposites using a soft lithography technique. In the first study, polymeric microtubular platforms are adorned with ZnO-Au hybrid nanowires designed for rhodamine B (Rh-B) dye degradation. Subsequently, in the next study, these microtubular platforms are fabricated with a nanopatterned structure and decorated with ZnO-Ta nanocomposites, enabling the real-time degradation of methylene blue (MB) dye solutions.

6.1 SUPERHYDROPHOBIC ZnO-Au NANOCOMPOSITE BASED POLYMERIC TUBES FOR PHOTOCATALYTIC DYE DEGRADATION

This work proposes a facile fabrication approach of a polymeric functional platform for rhodamine B (Rh-B) degradation. Herein, ZnO-Au nanohybrid wires have been synthesized with robust microfabrication approaches over the PDMS tubes. ZnO-Au hybrid wire increased the contact angle on the surface of the tube to 154.5° leading to a superhydrophobic surface. These synthetic nanocomposites are successfully tested for photocatalytic applications and evaluated the photocatalytic characteristics of ZnO nanowires and ZnO-Au hybrid wires. The super hydrophobicity of the resulting structure paved the way for its use in "self-cleaning" water treatment systems.

6.1.1 Introduction

Pigments and dyes are widely employed in a wide range of industries to generate correct colors for analytical purposes such as in biological laboratories as well as in manufactured products. Rh-B dye is a bright pink-colored synthetic dye used in paints, leather, textiles, laboratories, and food processing. When Rh-B is released into the aquatic environment, it creates very toxic and opaque wastewater. It is not only irritating to the skin, eyes, and respiratory tract, but also its exposure is very poisonous to the nervous and reproductive systems. As a result, this pollutant must be eliminated from wastewater in order to safeguard both the humans and environment. Further, the attractive properties of the hydrophobic solid surfaces have also been explored in a variety of applications, such as medical, electronics, paint, coatings and textiles, and a variety of other industries (Saharudin et al., 2018). Some possible applications include anti-corrosion coatings, waterproof textiles, and self-cleaning glass. In general, to avoid changes in textile qualities, hydrophobic textiles are made by intentionally treating textiles with low surface energy materials (Chen et al., 2009). Among various polymers, polydimethylsiloxane substrate (PDMS) has strong ductility and biocompatibility, so it meets many requirements for flexible device development (Sheshkar et al., 2021a). However, even PDMS has certain limitations. Flexible devices must be able to withstand various deformations when working at different temperatures. Therefore, studying the structural strength of flexible devices is essential to meet the needs of engineering applications. Due to their many attractive properties, nanostructured inorganic materials such as TiO_2, CeO_2, ZnO, and SnO_2 have been successfully applied to various surfaces to create new hydrophobic applications (Georgekutty et al., 2008; Gupta et al., 2013; Jing et al., 2013). The high functionality of these semiconductor oxides is crucial in several applications. Due to its remarkable characteristics and unique structure, the one-dimensional (1-

D) morphology of zinc oxide nanostructures such as nanowires, nanorods, and nanotubes, has received extensive attention (Gupta and Bhattacharya, 2018).

Fabrication via an aqueous chemical route is one of the simpler techniques available for manufacturing nanostructures. ZnO nanoparticles with controllable properties have recently been reported which is based on the chemical reaction between zinc acetate and some hydroxyl ions (OH^-) containing compounds, such as NaOH, KOH, etc. In some cases, nanostructure growth requires complex reactions, high temperatures, and sophisticated equipment (Bhattacharya et al., 2018a). The role of the reactants, their reaction temperature, and concentration have also been established in the formation of ZnO particles. The time and method by which the reagents are mixed also affect crystal growth and nucleation. Semiconductor nanomaterials for heterogeneous photocatalytic applications have emerged as significant emerging technologies, resulting in the complete mineralization of various organic pollutants and the production of ecologically favorable end products. The ability of the process to convert pollutants directly at the source into harmless substances is interesting (Dong et al., 2016; Laurenti et al., 2020).

In photocatalytic systems, photo-induced reactions occur at the surface of the catalyst. When the photocatalyst is illuminated with a light stronger than the energy gap ($h\upsilon \geq E_g$), the photocatalyst creates electron/hole pairs with free electrons (e^-) generated in the empty conduction band and leaves holes (h^+) in the valence band. Electron-hole pairs diffuse onto the photocatalytic surface and initiate a series of chemical reactions according to a commonly proposed mechanism. Recently, metals adsorbed on ZnO nanostructures were employed to extend ZnO's spectrum response to visible light. Chen et al. used photochemical deposition whereas Georgekutty et al. used a non-aqueous method for the deposition of silver (Ag) on ZnO for the synthesis of Ag-ZnO composite, and further investigated the photocatalytic applications (Chen et al., 2011; Georgekutty et al., 2008). The Schottky barrier between ZnO and Ag promotes charge separation and increases the efficiency of the degrading process (Deng et al., 2012). Ag can capture photogenerated electrons from the semiconductor, allowing holes to produce hydroxyl radicals, which can then react with organic molecules to degrade them. However, the majority of described procedures include the use of hazardous chemicals, the release of which into the environment is a significant source of concern. As a result, there is a rising demand for a novel technique for the manufacture of metal-metal oxide nanocomposite for dye degradation applications.

6.1.2 Material and methods

Commercially available chemical reagents such as zinc acetate dehydrate ($Zn(CH_3COO)_2 \cdot 2H_2O$), potassium hydroxide (KOH), methanol (CH_3OH), zinc nitrate ($Zn(NO_3)_2$), hexamethylenetetramine (HMTA), Rhodamine B (Rh-B) dye was purchased from (Sigma Aldrich). All chemicals utilized to perform the experiments were of AR grade. The PDMS tubes are prepared from the two-part kit containing a Sylgard 184 (elastomer base), and curing agent (cross-linker) was procured from (Dow Europe GMBH CIO DOW SILICONES, GERMANY).

(a) Fabrication of PDMS tube

The Sylgard 184 and the curing agent were mixed in a 10:1 ratio. After that, a degasification technique was adopted to eliminate all of the air bubbles that developed during the mixing process. Degassed PDMS was then poured into the plastic tubular template (2 mm diameter) and were kept at 70°C for 6 hours in a furnace to cure. The tubular template is then cut carefully to remove the 2 mm diameter PDMS tubes.

(b) Synthesis of ZnO nanoparticles via Sol-gel method

In this technique, 0.016 M KOH was dissolved in CH_3OH and heated to 65°C. Afterward, the mixture was vigorously stirred for 25 min to obtain a homogeneous solution. Another solution of 0.01M $Zn(CH_3COO)_2 \cdot 2H_2O$ in DI water was prepared. Finally, both the solutions are added together (Z1) and were rapidly stirred at 60°C for 90 min. In order to obtain the nanoparticles, the

prepared (Z1) solution is centrifuged at 5000 rpm for 5 min followed by rinsing 3-4 times with DI water and methanol.

(c) Deposition of ZnO around the PDMS tubular substrate

The procedure of growing ZnO nanostructure on polymeric substrates using the process described below allows the growth of NWs over large areas in an environmentally friendly and simple manner. The prepared ZnO nanoparticle is ultrasonicated with isopropyl alcohol for 1 hour to obtain a homogeneous solution. The ultrasonication was continued until the solution became milky white. PDMS tubes were properly rinsed with distilled water and then acetone, then the solution is drop cast and spray-coated over the tube for the initial growth. After that, the tube was baked on a hot plate at 90°C. This procedure was repeated multiple times to achieve a uniform layer thickness of seeded ZnO over the PDMS tube.

(d) Fabrication of ZnO nanowire over the seeded substrate

To accelerate the growth of ZnO NWs, the substrate with a high-density seed layer was used. Then, a solution containing $Zn(NO_3)_2$ and HMTA in a ratio of 1:5 in distilled water was used for the growth step. The ultrasonication technique was used to homogenize the solution. The substrates (PDMS tubes) were submerged in the solution for 10 hours at 95°C. Structural characterization was performed using FESEM to investigate the morphology and size of the generated ZnO nanowires. A succession of chemical reactions leads to the formation of ZnO nanowires on a substrate surface. In the presence of heat, HMTA hydrolysis in solution and generates ammonia (NH_3) and formaldehyde ($HCHO$). The released NH_3 promotes the production of hydroxyl ions $OH^-$and inhibits significant numbers of Zn^{2+} from forming in solution (Chauhan et al., 2019). Ammonia is broken down further into NH_4^+ and OH^-. The complex chemical $Zn(OH)_4^{2-}$ is formed when OH^- reacts with Zn^{2+}. Under reaction conditions, it dehydrates to produce nanowires. After the growth of ZnO nanowires, sputtering was carried out in an Ar plasma at 1.6 Pa operating pressure with 100 W sputtering power, and the target substrate was kept at 10 cm. The sputtering time ranged between 10 and 25 mins. The sample was then annealed for 25 mins at 350°C in a muffle furnace. After that, the sample was immersed in ethanol for 15 min before being dried at 95°C for an hour. The FESEM images show the presence of Au over the grown ZnO nanowires.

6.1.3 Results and Discussion

(a) Structural Characterization

The surface morphological characteristics of all samples were studied using a FESEM (Carl Zeiss), and EDS (Oxford instruments). At an accelerating voltage of 20 kV, the images were obtained at magnifications ranging from 5kX to 50kX. Figure 6.1 depicts the FESEM image of (a) ZnO NPs, (b) ZnO seed layer, (c) ZnO NWs, and (d) Au sputtered ZnO NWs over PDMS substrate. Au is deposited with the help of the Sputtering method, ~100nm deposition is carried out over ZnO NWs. Figure 6.1 (e, f) shows the EDS results. Because of its small size, the seed had high surface energy. As previously stated, after a thin, uniform film of finely distributed seeds was applied to the surface of the substrate and submerged in the growth solution, Zn^{2+} and O^{2-} ions are attracted to the seeds, decreasing the surface energy. Because of the optimal temperature for growth (Chauhan et al., 2017), these ions have enough energy to unite and arrange themselves in the (002) direction with the hexagonal structure. As a result, one-dimensional polycrystals in the form of nanowires were formed. Nanowire with finely distributed seeds has enough free space for compact growth of smaller diameters due to the presence of HMTA that impede lateral progression. Furthermore, the ability of any substrate to support a homogenous distribution of the layer of nano seeds is associated with the formation of ZnO NWs. The characteristics of the surface of the substrate have a considerable impact on the applied layer deposition, which supplies growth nucleation sites (Biswal et al., 2021). By providing sufficient nucleation sites, the nano-seeds coating helps to minimize these thermodynamic barriers. It has also been shown that

pre-heating of the substrate at a temperature of 300-350°C is not essential for zinc acetate decomposition. The growth of well-ordered nanowires was obtained at a temperature of about 90-95°C. The nanorod length increases as the temperature increases due to faster ion mobility and diffusion (Liu and Zeng, 2003; Ridhuan et al., 2012).

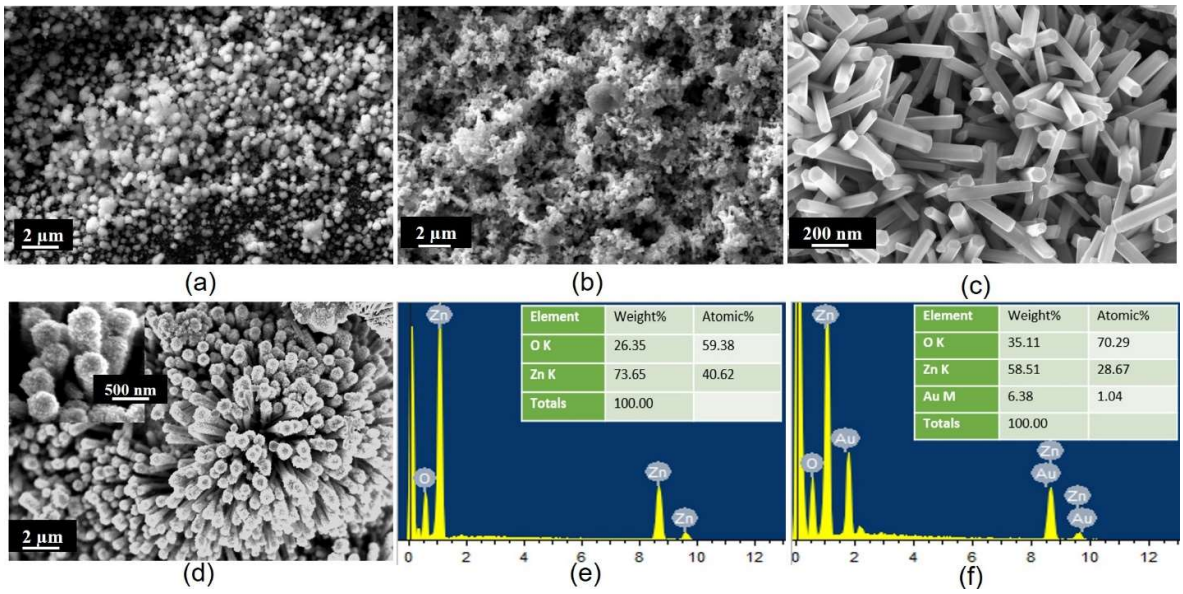


Figure 6.1. FESEM image of (a) ZnO NPs (at 5kX), (b) ZnO seed layer (at 5kX), (c) ZnO NWs (at 50kX), and (d) Au sputtered ZnO NWs (at 5kX) over PDMS substrate, and (e-f) EDS results of ZnO and ZnO-Au hybrid wires

(b) Contact angle and surface free energy measurement

In the current work, due to the presence of Au-ZnO composite over to the PDMS tube, the contact angle has increased as compared to pure PDMS. The contact angle is measured using the instrument (Kruss DSA25B). The surface tension of a liquid is caused by the fact that a molecule near the surface has fewer surrounding molecules with which it can interact as compared to the bulk of the liquid. This is why liquids try to have the smallest possible surface area. The SFE of solid phases is treated similarly in theory. In contrast to the bulk phases, it is difficult to directly determine the amount of work necessary to enhance a surface area of solid. As a result, the idea of contact angle (θ) is developed to measure the wettability by liquid to determine the SFE of a solid. Young's equation helps describe the wetting phenomenon on a macro scale as shown by the following equation,

$$\gamma_{lv} cos\theta = \gamma_{sv} - \gamma_{sl} \tag{6.1}$$

Where, γ_{sl} , γ_{sv}, γ_{lv} , are represented as the energy required for the solid-liquid interface, the solid-vapor interface, and the liquid-vapor interface, respectively. The surface represents wetting and non-wetting states when the contact angle is 0° and 180°, respectively. When the contact angle of the surface reaches <90°, it is known as hydrophilic, and when it reaches >90°, it is known as hydrophobic. Based on the fundamental interactions between molecules, Owens, Wendt, Rabel, and Kaelble (OWRK) technology produces a two-component model that differentiates interfacial tensions. These interactions are polar and dispersion interactions and the sum of these interactions is known as the total surface energy of the solid. Permanent dipole-permanent dipole interactions are the basis of polar interactions and exist only in polarity, whereas the dispersion component is weak and is caused by the variations in the electronic cloud resulting in transient dipole interactions. SFE for example, γ_{sl} and γ_{sv} are the two unknown variables in the OWRK approach. Calculating these variables requires at least two liquids with known polar and dispersed surface tensions. The following equation gives the OWRK model.

$$\gamma_{sl} = \gamma_{sv} + \gamma_{lv} - 2(\sqrt{\gamma_{sv}^{P}\gamma_{lv}^{P}} + \sqrt{\gamma_{sv}^{D}\gamma_{lv}^{D}}) \quad (6.2)$$

Where, γ_{sv}^{P}, γ_{sv}^{D} represent the surface energies of solid and γ_{lv}^{P}, γ_{lv}^{D} represent the liquid surface energies of its polar and disperse components, respectively. Further solving the equation (11), gives

$$\sqrt{\gamma_{sv}^{P}\gamma_{lv}^{P}} + \sqrt{\gamma_{sv}^{D}\gamma_{lv}^{D}} = \frac{[\gamma_{sv}+\gamma_{lv}-(\gamma_{sv}-\gamma_{lv}\cos\theta e)]}{2} \quad (6.3)$$

$$\sqrt{\gamma_{sv}^{P}\gamma_{lv}^{P}} + \sqrt{\gamma_{sv}^{D}\gamma_{lv}^{D}} = \frac{[\gamma_{sv}(1+cos\theta e)]}{2} \quad (6.4)$$

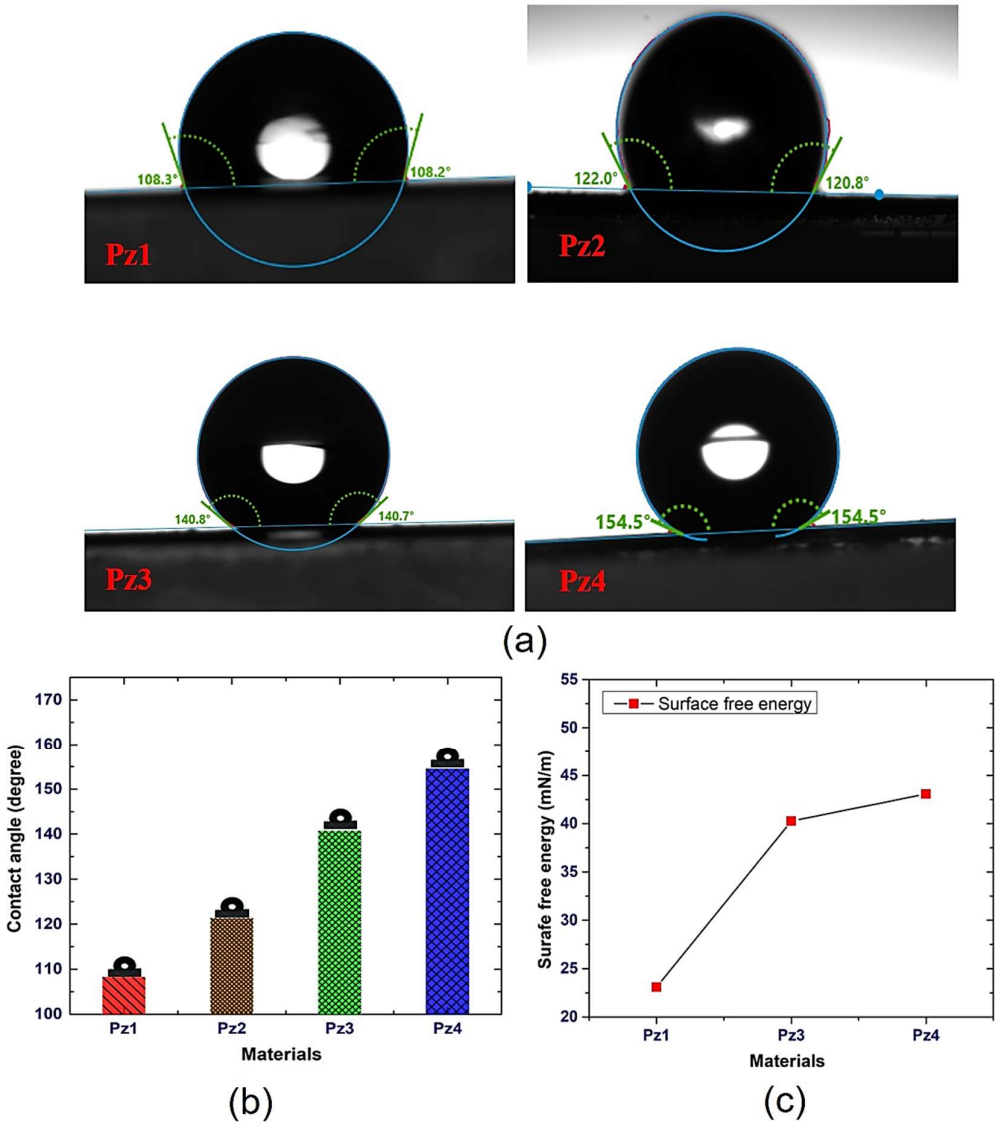


Figure 6.2: Contact angles results of (a) Pz1- pure PDMS (CA: 108.25°), (b) Pz2- PDMS/ZnO seed (CA: 121.4°), (c) Pz3- PDMS/ ZnO NWs (CA: 140.75°), and (d) Pz4- PDMS/ZnO-Au (CA: 154.5°), and (b, c) Relation between contact angle, Surface free energy and materials (Pz1, Pz2, Pz3, and Pz4)

A superhydrophobic surface must have a hierarchical nano roughness as well as low surface energy. The growth of the ZnO-Au nanohybrid wires helps in generating the nano roughness and low surface energy which will surfaces aids in the trapping of large amounts of air and the reduction of the solid-liquid interface, increasing the contact angle of the produced ZnO-Au surface and decreasing the tendency of water to bond with the surface. When the contact

angle is lesser than 90°, the surface is well wetted and the liquid will spread over a large area of the surface, however, when the contact angle is greater than 90°, the surface is poorly wet and the liquid is reducing contact with the surface to generate droplets. The standard definition of contact angle is the angle formed when a liquid is placed on a liquid or solid surface. The larger the contact angle, the greater is the cohesion, and the liquid molecule's interactions among themselves are frequently more in contrast to the interaction between the solid molecules. Thus results show that the cohesiveness of the ZnO-Au composite is significantly better than the adhesion of pure ZnO due to the increased contact angle. Figure 6.2 (a-d) shows the results of the contact angle. The graphical relation of contact angle vs material and SFE vs material is shown in Figure 6.2 (e, f). Tables 6.1 and 6.2 show the properties of probe liquid and the value of coS1ntact angle and surface free energy of different samples, respectively.

Table 6.1: The properties of probe liquid used to measure surface free energy at 20°C

Probe Liquid	Polar*	Disperse*	SFT*
Water	51	21.8	72.8
Toluene	2.3	26.1	28.4

* All values are in mN/m

Table 6.2: Contact angle and SFE results of various samples

Material	CA (Θ°)	Total SFE*	Disperse SFE*	Polar SFE*
Pz1	108.3°	23.08 ± 0.42	22.95 ± 0.34	0.12 ± 0.08
Pz3	140.75°	40.26 ± 0.38	29.75 ± 0.15	6.43 ± 0.23
Pz4	154.5°	43.06 ± 0.12	33.86 ± 0.05	9.20 ± 0.08

* All values are in mN/m

(c) Photocatalytic degradation

To insert the PDMS tube's base and expose the outer surface to the Rh-B solution, an acrylic container with a drilled hole in the base was developed. A 200 mL aqueous solution with a concentration of 10 mg L^{-1} was added to the tank, and the mixture was occasionally agitated by hand. Two PDMS tubes, each 2 mm in diameter and 3 cm in length, were thickly covered with ZnO nanowires and immersed in a solution of Rh-B dye. The experiment was carried out in a dark room, and the setup was subsequently irradiated to 5 W of UV light. The solution was stirred in the dark for 2 hours before irradiation to achieve adsorption-desorption equilibrium. To assess the rate of degradation, a 5 mL sample of the mixture is drawn at regular intervals to record the UV–visible absorption spectra. Figure 6.3 illustrates the experimental setup with the PDMS tube immersed in Rh-B solution.

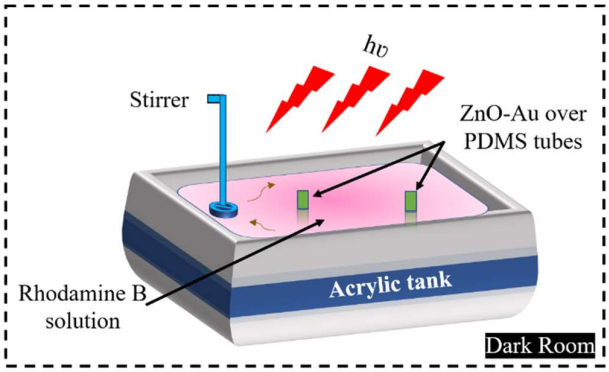


Figure 6.3: The schematic of the experimental setup used for the degradation of Rh-B solution

Photocatalytic investigation of ZnO-Au composite grown on PDMS tubes

Under UV-light exposure, the effect of Au sputtered ZnO composite on the decoloration of Rh-B was investigated. Within 330 min of observation, the position and maximum intensity at 554 nm remained stable under dark conditions. Figure 6.4 (a-b) depicts, the maximum peak at 554 nm decreased significantly as the exposure time of UV light increased in each case. The reduction in 554 nm emission intensity was attributable to Rh-B degradation under UV-light exposure, and so the manufactured ZnO-Au composite over PDMS tube showed strong photocatalytic reactivity for Rh-B degradation. Figure 6.4 (c), the fitting of the normalized maximum absorbance to time reveals a degradation. According to the Beer-Lambert rule, which stipulates that there is a linear relationship between the concentration and absorbance of the solution, the normalized concentration of the Rh-B solution takes the place of the normalized absorbance (Kumar et al., 2021b). The photocatalytic action of these samples annealed at different temperatures (300°C and 500°C) has been investigated. The degradation time of Rh-B dye was improved by annealing at 300°C and 500°C to 430 and 400 mins, respectively. As a result, as illustrated in Figure 6.4 (c), the degradation characteristic of Rh-B follows pseudo-first-order kinetics. The slope value of ZnO-Au is higher than all the samples indicating the higher rate constant.

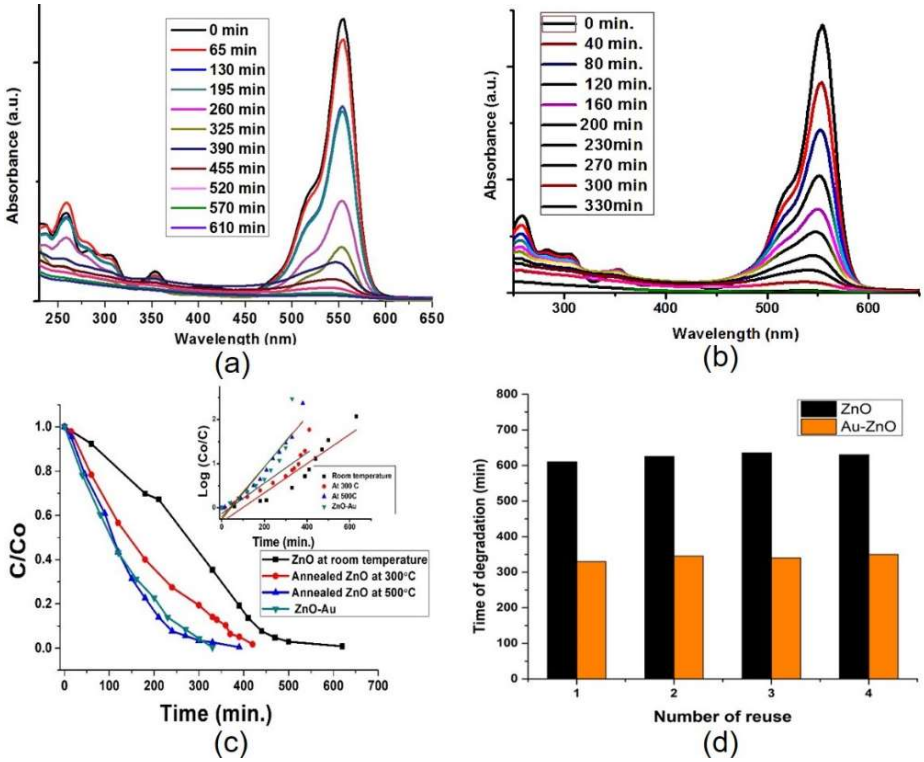


Figure 6.4: UV vis absorbance spectra of (a) ZnO NWs, (b) ZnO-Au hybrid wires, for photocatalytic degradation, (c) experimental and kinetics of photodegradation of Rh-B dye, and (d) reusability curve using the dye degradation time vs the number of usage

Reason for enhancement in the photocatalytic activity with ZnO-Au

ZnO-Au composites absorb 366 nm UV light and transfer more electrons from lower energy levels to higher energy levels. Resulting in the generation of more photogenerated charge carriers, which are responsible for dye decoloration. UV-induced conduction electrons interact with -OH groups in an aqueous solution to produce -OH radicals, as illustrated in the equation below. The -OH species react with Rh-B molecules, causing Rh-B groups to chemically cleave and the dye to degrade (Natarajan et al., 2011; Subramanian et al., 2003).

$$ZnO \xrightarrow{UV} e_{CB}^{-} + h_{VB}^{+} \tag{6.5}$$

$$O_2 + e_{CB}^- \rightarrow O_2^- \quad (6.6)$$

$$O_2^- + e_{CB}^- + 2H^+ \rightarrow H_2O_2 \quad (6.7)$$

$$H_2O_2 \rightarrow 2\,(\cdot OH) \quad (6.8)$$

$$h^+ + OH^- \rightarrow \cdot OH \quad (6.9)$$

$$h^+ + H_2O \rightarrow \cdot OH + H^+ \quad (6.10)$$

$$\cdot OH + RhB_{ads} \rightarrow Degraded_{product} \quad (6.11)$$

Two possible mechanisms of Rh-B degradation were identified: (a) de-ethylation, a stepwise adsorption dye on the surface of the negatively charged catalyst, which causes a shift in the characteristic UV absorption peaks, and (b) the chromophore xanthene group due to the adsorption of the dye by -COO on the surface of the positively charged catalyst. This serves to separate the chromophores that cause the color of the dye. This cleavage causes discoloration of the dye and manifests itself in a significant decrease in UV peak intensity. Similarly, the energy band structure of the Au-ZnO composite was examined in an attempt to determine why photocatalytic activity improved. The work functions of Au and ZnO are reported to be 5.2 and 5.1eV, respectively (Perumal et al., 2016), indicating that Au has a higher Fermi energy level than ZnO. After Au is deposited on ZnO nanowires, electrons move from Au to ZnO to align the Fermi energy level at equilibrium. This behavior causes the band edge of ZnO to shift upwards, resulting in band bending at the contact. As a result, ohmic contact between ZnO and Au is formed, and the energy band structure is illustrated in Figure 6.5. The formation of an ohmic contact creates a channel for electron transmission from the higher energy level of ZnO (conduction band) to the lower energy level of Au (Fermi level) (Lee et al., 2011). The electrons migrated to Au as soon as they were stimulated into the conduction band of ZnO by UV irradiation. This method successfully separates photogenerated carriers, hence improving the photocatalytic activity of the ZnO-Au composite. During this procedure, no movement in UV peak position was noticed, however, all samples analyzed showed a drop in absorption peak intensity. As a result, it can be concluded that the cleavage of the xanthene group is the primary mechanism in all degradation experiments. Figure 6.6 depicts the possible degradation mechanism of Rh-B dye over ZnO-Au composite. To test the cycling behavior of the Au-ZnO composite, we conducted an experiment. For ZnO, cycles 1-4 took 610, 625, 635, and 630 min while for ZnO-Au, cycles 1-4 took 330, 345, 340, and 350 min respectively. Figure 6.4 (d) represents the dye degradation time is shown against the number of usage. Previous work on ZnO-based composites for photocatalytic applications has been provided in the form of a comparison Table 6.3.

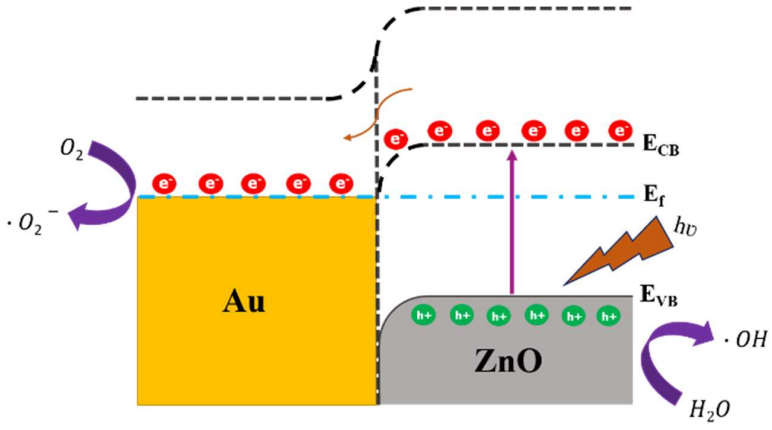


Figure 6.5: The possible reaction mechanisms over of Au/ZnO under UV irradiation

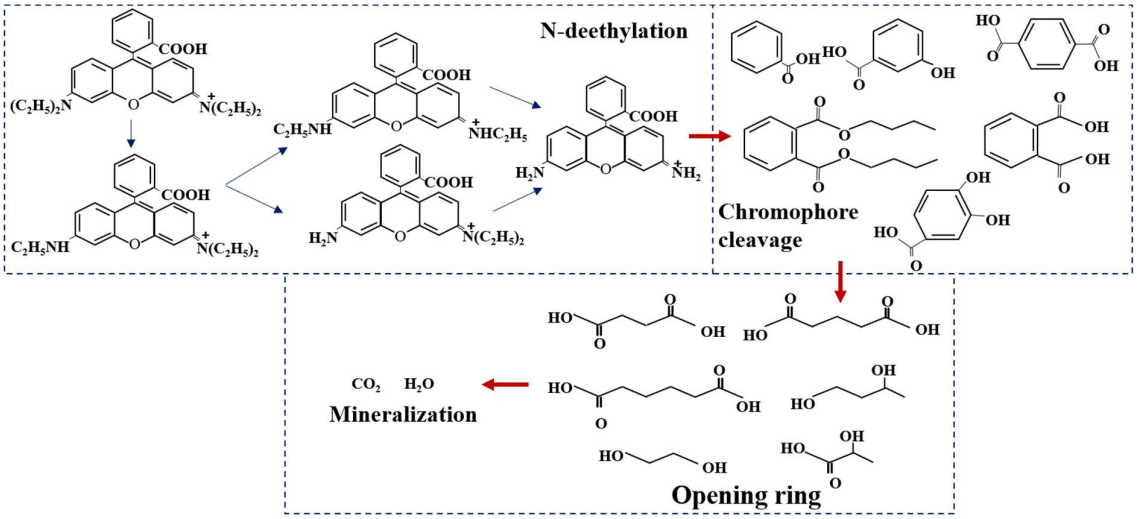


Figure 6.6: Possible Rh-B dye degradation process in an Au/ZnO composite

Table 6.3: Previous work on ZnO-based composites for photocatalytic applications

Material	Dye solution	Light source	Irradiation time	Dye	Reference
Fe/ZnO	10 mg/L	UV light	180 mins	Rh-B	(Yi et al., 2014)
Nanoporous ZnO	5 ppm	Sunlight	260 mins	MB	(Zayed et al., 2019)
ZnO NPs	33.46 mg/L	Sunlight	180 mins	RhB	(Byrappa et al., 2006)
ZnO/Au/Ag	-	Visible light	360mins	phenol	(Fageria et al., 2014)
Ag/Cr/Pb/Mn doped ZnO	-	UV light	300 mins	RhB	(Le and Pung, 2021)
ZnO/SnO_2 nanofibers	0.01 mM	Visible light	360 mins	RhB	(Pascariu et al., 2016)
ZnO and TiO_2	-	Sunlight	420 mins	Acid brown 14	(Sakthivel et al., 2003)
ZnO/Au/PDMS	10 mg/L	UV light	330 mins	Rh-B	Present work

6.1.4 Summary

We offer a promising method for fabricating a tube employing non-toxic and biocompatible PDMS materials and growing ultrahigh nanostructures of ZnO and ZnO-Au hybrid wires, which can surely deliver a greater number of active sites for many applications. For the formation of ZnO-Au composite, these PDMS tubes were responsible for delivering a high surface-area-to-volume ratio. The dense growth of the Au sputtered ZnO NWs was confirmed by FESEM studies. Further, the superhydrophobic nature of the fabricated structures has opened a new avenue for utilizing them for "self-cleaned" water treatment systems. The entire degradation of the dye took ~330 mins with the ZnO- Au hybrid wires coated PDMS tube. Thus, ZnO-Au hybrid wires have made the photocatalytic reaction faster than ZnO wire. The photocatalytic degradation effect of Au-ZnO hybrid wires can improve high-density active sites for the chemical reaction of dye degradation, along with the increased charge separation. This investigation will

assist researchers in better grasping the relationship between photocatalyst structure and activity. The effect of this catalyst on the degradation of genuine industrial wastewater containing organic contaminants should be explored in future investigations. These high-quality ZnO-Au structures can be the idyllic choices for low-dimensional physics research and applications at the nanoscale level in a variety of scientific and technical domains.

6.2 REAL-TIME DEGRADATION OF METHYLENE BLUE USING BIO-INSPIRED SUPERHYDROPHOBIC PDMS TUBE COATED WITH Ta-ZnO COMPOSITE

In this work, the synthesized tantalum (Ta)-doped Zinc oxide (ZnO) composite coated over the bioinspired polymeric platform has been reported for the decolouration of methylene blue (MB) dye when exposed to UV light. The contact angle results show the contact angle of 108˚ for pure polydimethylsiloxane (PDMS) and 168˚ for bio-inspired PDMS with Ta-doped ZnO composite leading to a superhydrophobic surface. This superhydrophobic bio-inspired polymeric platform was modified by optimizing the surface roughness and coating it with low-surface-energy Ta-ZnO NWs composites, paving the way for it to be envisioned in "self-cleaning" water treatment facilities. These photocatalysts lead to "waste control using Ta-ZnO NWs composites," which opens up new possibilities for flexible and biocompatible environmental remediation platforms. In this study, real-time MB dye degradation is also monitored using the Internet of things (IoT) technique by integrating a NodeMCU microcontroller board as a control center and a pH sensor as a tool for detecting the change in pH value of the MB dye under UV light exposure.

6.2.1 Introduction

The chemical business makes extensive use of color. However, the usage of paints in industry is rapidly growing, the resulting in increased the natural water contamination. In fact, even extremely little level of dye in the water (as little as 1 mgL^{-1} for certain dyes) is visible and enough to cause aesthetic issues. Organic chemicals, such as dyes, are toxic to humans (Rai and Gupta, 2022). It is believed that about 15% of all dyes produced in the world are discarded in the dying and printing operations, and this waste is released into the water. As a result, innovative wastewater treatment technologies are always needed to address environmental contamination. Traditional techniques for wastewater decontamination have been used for decades, including adsorption, coagulation, the Fenton process, flocculation, aerobic treatment, heterogeneous photocatalysis, reverse osmosis, precipitation, ozonation, membrane filtration, and many more (Chauhan et al., 2022). These traditional technologies, however, are inefficient in wastewater treatment and reuse owing to several restrictions such as expensive chemical and operating expenses, advanced processes, complicated sludge production, separation challenges, long process times, and many more. Photocatalysis is a potential approach for eliminating organic pollutants without producing secondary pollutants that require additional treatment. Different metal oxide semiconductors are thought to be potential photocatalysts such as ZnO, TiO_2, SnO_2, WO_3, etc., for converting organic pollutants to ecologically favorable species (Gupta et al., 2014, 2013; Gupta and Bhattacharya, 2018; Mulay et al., 2019; Singh et al., 2019). Because of its photosensitivity, nontoxicity, and lower price than precursors, ZnO is a potential semiconductor for photocatalytic applications. The wide bandgap and higher recombination rate of photoexcited electron-hole pairs are the major disadvantages that prevent ZnO nanoparticles from being used in industry. A literature analysis also revealed that due to faster electron and hole recombination, undoped ZnO has only limited photocatalytic effectiveness. As a result, some method of slowing recombination and increasing the number of charge carriers is required. To improve the performance of ZnO, the technique of doping specific appropriate metal ions is used. Transition metals such as Ag, Co, Ce Cu, Cr, Mn, Mo, Ni, Ta, and V, have been doped into ZnO to change their properties (Chauhan et al., 2018a; Chen et al., 2018). Tantalum (Ta) is one of the suitable doping metals for ZnO, with an ionic radius of 0.064 nm (Ta^{5+}) that is similar to that of 0.074 nm

(Zn^{2+}). When compared to other transition metals, Ta is the most effective dopant for boosting ZnO photocatalytic ability (Chennakesavulu et al., 2015; Kong et al., 2010). Most industrial wastewater contains methylene blue (MB), the most prevalent color in effluent from the fabric, sheet, and printing companies. It is difficult to eliminate MB from the wastewater due to the existence of an aromatic ring structure that contains polar groups and chromophores. Many researchers are working to eliminate MB by adsorption by lotus leaves (Han et al., 2011).

In recent years, superhydrophobic surfaces having more than 150˚ water contact angle (WCA) have piqued academic and industrial attention. For many applications, having unique features is crucial such as biocompatibility, self-cleaning, water repellency, improved material durability, and other features to avoid contamination (Lin et al., 2011). The chemical composition and morphological features present on a surface are considered to influence super hydrophobicity (Li et al., 2007). In nature, there are a lot of plants that have hydrophobic surfaces. The air was trapped as a cushion for the water droplets that dropped on the leaf due to the hierarchical micro/nanostructures, resulting in superhydrophobicity. In this study, we have attempted to develop lotus leaf-like superhydrophobic structures on polydimethylsiloxane (PDMS) substrate and to examine its photocatalytic ability to degrade MB dye when coated with Ta-ZnO composite. Because of its ductility and biocompatibility, the PDMS substrate is ideal for flexible and stretchable platform (Sheshkar et al., 2022, 2021a). Therefore, it has a wide range of applications. Industrial wastewater, mostly from chemical and pharmaceutical processing, frequently contains contaminants that must be treated before being discharged. The effect of not adhering to the standard disposal of dyes is that water with an uneven acidity level would disrupt the environment's health and ecology. Manual collection of water samples at various sites is used in traditional water quality procedures, which are then analyzed in laboratories to identify the character of water. The procedure will result in certain errors, such as the worker entering incorrect data. Therefore, in this study, real-time MB dye degradation is monitored using the IoT technique. We have a monitoring system based on the NodeMCU microcontroller development board as a control center and a pH sensor as a tool for detecting the change in pH value of the Textile dye.

6.2.2 Material and methods

Sigma-Aldrich provided zinc acetate dihydrate ($ZnC_4H_6O_4$), potassium hydroxide (KOH), methanol, zinc nitrate, hexamethylenetetramine (HMTA), isopropyl alcohol (IPA), Slygard 184, and curing agent and methylene blue dye. All of the chemicals utilized were AR grade, and they were used exactly as they were received, with no further purification.

(a) Fabrication of superhydrophobic PDMS tube

The PDMS prepolymer (Slygard 184) and curing agent were mixed in a 20 mL beaker in a 10:1 ratio before being placed in a vacuum desiccator to remove any air bubbles that form during the mixing process (see Figure 6.7). After 30 mins of degassing, PDMS was poured into 2 mm diameter plastic tubes which are placed vertically. Now, a copper wire with a diameter of 1.0-1.25 mm is inserted vertically into the PDMS-filled tubular template and cured in an electric oven at 80°C for 5 hours. The 2 mm diameter PDMS tubes are then carefully removed from the tubular template. Now, for the removal of copper wire, the whole PDMS tube was dipped in chloroform for 30 secs. The chloroform allows PDMS to swell and copper wire will be easily removed by applying a light mechanical pulling force. Finally, the hollow PDMS tube can be obtained. For bio-mimicking the structure of the lotus leaf on PDMS, a fresh lotus leaf is taken and cleaned thoroughly and dried. A thin layer of PDMS was applied over the leaf using a brush, and a fabricated PDMS tube was wrapped around the leaf and placed in an electric oven at 65°C for 60 mins to cure.

(b) Growth of Ta-ZnO composite over the PDMS tubes

The synthesis of Ta-ZnO composite starts with the seeding of PDMS tubes with ZnO and Ta-ZnO nanoparticles (NPs). For preparation of Ta-ZnO seed, 3 g of $Zn(CH_3COO)_2(H_2O)_2$ were

dissolved in 62.5 mL of isopropyl alcohol and 93 mg Ta_2O_5 in 25 mL of glacial acetic acid. In a 100°C hot plate, both solutions were combined and magnetically agitated for 60 min. Pure ZnO reference samples were simultaneously synthesized using the same procedure but do not contain the Ta_2O_5 precursor. Both the prepared NPs were used to further seed the PDMS tubes. The prepared PDMS tubes were cleaned with acetone and DI water, then dip-coated in both seed solution one by one, for the initial growth of the ZnO and Ta-ZnO seed layer, and finally calcined at 70°C in an electric oven. A high-density and the uniform ZnO seed layer was preferred to accelerate the growth of the Ta-ZnO NWs. Now, in a 500 mL beaker, a homogeneous solution containing $Zn(NO_3)_2$ and HMTA (1:5) was prepared in DI water using a probe sonication technique. The ultrasonication technique was used to homogenize the solution. In a separate beaker, a Ta_2O_5 solution was made by dissolving 0.2 g of Ta_2O_5 in 20 mL ethanol and then ultrasonicated for 180 mins. Then, 4 mL of Ta_2O_5 solution was added to the previously prepared $Zn(NO_3)_2$ - HMTA solution. After that, seed PDMS tubes were placed in the solution for 8 hours at 90°C. Finally, the Ta-ZnO composite is deposited on the PDMS tube. Similar technique was used to growth Ta-ZnO nanocomposite using the Ta-ZnO seeded PDMS tubes, but this method led to the agglomeration of nanoparticles and the loss of the nanowire-like structures over the PDMS tubes.

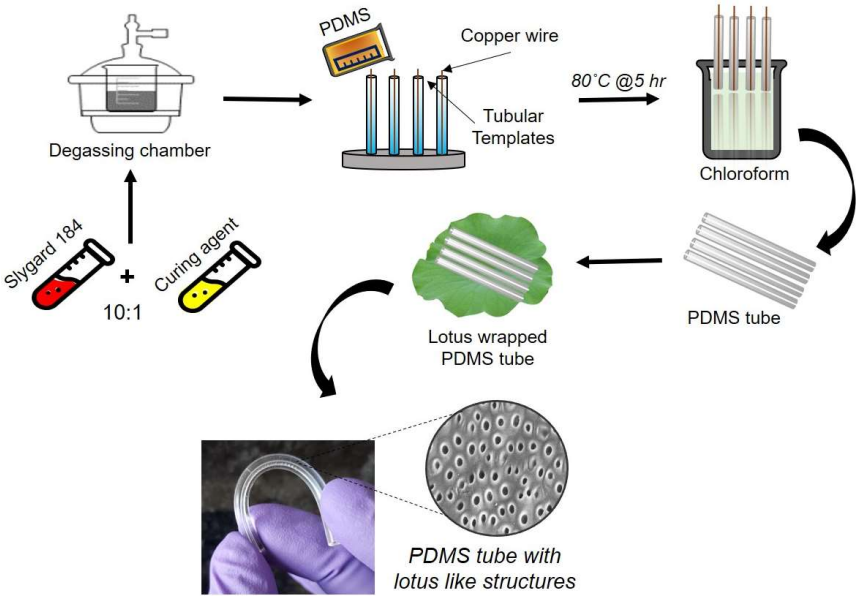


Figure 6.7: Schematic of fabrication of PDMS tube with lotus-like microstructures, with inset photograph of PDMS tube with an inner diameter of 1.15mm

6.2.3 Results and Discussions

(a) Surface Characteristics

An SEM (Carl Zeiss) and EDS (Oxford instruments) were used to examine the surface morphological features of all the synthesized specimens at an accelerating voltage of 10 kV. The SEM image of (a) lotus microstructure replicated PDMS (L-PDMS), (b) L-PDMS/ZnO seed layer, (c) L-PDMS/ZnO NWs, and (d) Ta-ZnO NWs coated over L-PDMS tube are shown in the Figure 6.8 (a-d). The presence of Ta and Zn can be evaluated by EDS results (see Figure 6.8 (e-f)). The surface energy of seed layer is high due to its small size. After the substrate is placed in the growth solution, a thin, homogeneous film of finely dispersed seed is attached to the PDMS substrate, enticed Zn^{2+} and O^{2-} ions to the seed, lowering surface energy. These ions have quite enough energy to unify and organize themselves in the <002> to form a hexagonal structure because of the optimal temperature for growth (Chauhan et al., 2017). 1-D polycrystals in the form of NWs were formed as a result. Because of the presence of HMTA, which impedes lateral progression, NWs with finely distributed seeds has enough free space for compact growth of smaller

diameters. In addition, the ability of any substrate to support a uniform distribution of nano seeds is linked to the formation of ZnO NWs. The properties of the substrate's surface have a huge influence on the film's deposit that provides growth nucleation sites (Biswal et al., 2021).

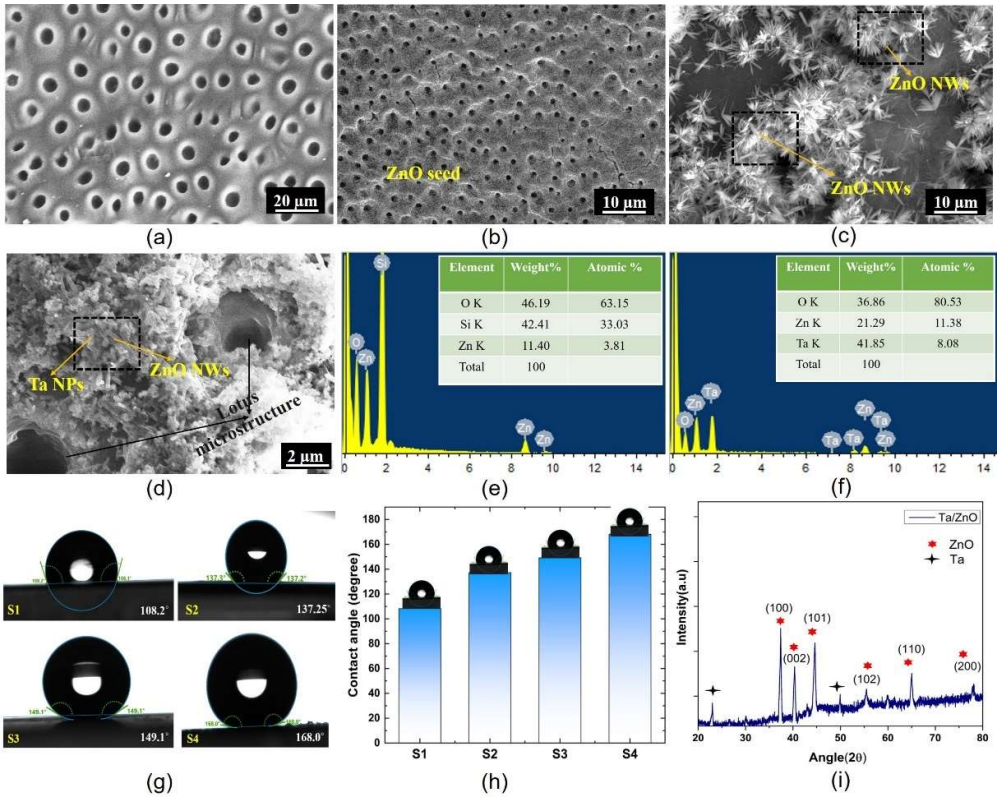


Figure 6.8: SEM image of (a) L-PDMS, (b) L-PDMS/ZnO seed layer, (c) L-PDMS/ZnO NWs, and (d) L-PDMS/Ta doped ZnO NWs, and (e-f) EDS results of a sample L-PDMS, and L-PDMS/Ta-doped ZnO, (g-h) Contact angles results of S1- pure PDMS (without lotus structure replications (CA: 108.3˚)), S2- L-PDMS (CA: 137.25˚), S3- L-PDMS/ZnO NWs (CA: 149.1˚), and S4- L-PDMS/Ta doped ZnO NWs (CA: 168.1˚), (i) XRD of Ta-ZnO composite

(b) Water contact angle (WCA) Results

The Kruss DSA25B instrument was used to predict the water contact angle (CA) of pure and Ta-ZnO coated PDMS tubes. The results show that as the Ta-ZnO composite over lotus microstructure-based PDMS tubes grows, the CA increases to 168.0° in comparison to pure PDMS tubes with a CA: 108.2°. Figure 6.8 (d) shows the results of the contact angle of various samples, (a) S1- pure PDMS (without lotus structure replications), (b) S2- L-PDMS, (c) S3- L-PDMS/ZnO NWs, and (d) S4- L-PDMS/Ta doped ZnO NWs. Table 1 shows the properties of probe liquid. OWRK technology has been used to develop a working model that distinguishes interfacial tensions based on the fundamental interactions between molecules. From the SEM results, the pore size space between the surface of NWs helps capture air, resulting in a decrease in the solid liquid interface, and thus increasing the CA of the Ta-ZnO NWs surface, according to SEM findings. According to the literature, if the CA is < 90°, the surface will be sufficiently wet and the liquid will spread over the entire surface, whereas, the surface will be poorly wetted and the liquid reduces its contact with the surface to produce droplets if the CA is > 90°. The greater the CA, the higher the cohesion and the interactions between liquid molecules are frequently more in contrast to those between solid molecules. As a result of the increased CA, the cohesiveness of the Ta-ZnO composite is significantly better than pure ZnO adhesion. Furthermore, the air was trapped as a cushion for the water droplets that dropped on the lotus-like structure with Ta-ZnO NWs composite due to the hierarchical micro/nanostructures, resulting in superhydrophobicity of up to 168°. Figure 6.8 (g-h) depicts the graphical relationship between contact angle and material, as well as SFE and material.

(c) X-ray diffraction (XRD)

Figure 6.8 (i) depicts the XRD patterns of Ta doped ZnO films. The diffraction patterns were recorded in the 2θ range of 20-80° using Cu K1α radiation (1.54059 A°). The peaks of the hexagonal wurtzite phase of ZnO were identified and peak intensity matches with JCPDS card No. 00-036-1451 (Marouf et al., 2017). The XRD patterns corresponding to Ta-doped ZnO have the same characteristics as those found in undoped ZnO samples. After 200° of thermal treatment, we see the presence of the Ta_2O_5 precursor phase. The major peak of this phase is 2θ=23°. This is similar to the finding reported by Richard et al. (Richard et al., 2018). The influence of temperature on the XRD pattern of Ta-doped ZnO was further investigated by the author, who discovered that when the temperature rises, the peak of 2θ=23° decreases.

(d) Photocatalytic degradation of Ta-ZnO NWs composite grown over PDMS tubes

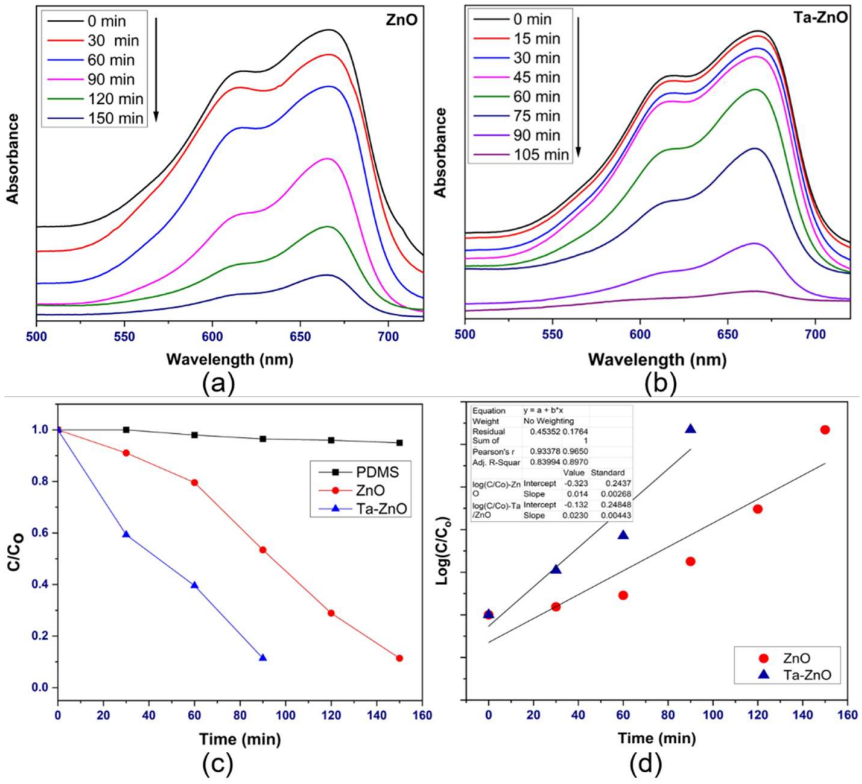


Figure 6.9: UV-vis spectrum of (a) pure ZnO, (b) Ta-ZnO composite, and (c, d) experimental and kinetics of photodegradation of MB dye

The photocatalytic efficiency of nanowires generated on the fabricated tubular hollow PDMS substrate was evaluated by analysing the rate of degradation of MB in an aqueous solution with UV radiation. To expose the Ta-ZnO/PDMS tubes to the 300 mL MB dye solution formed with a 10 mg L^{-1} (concentration), a small acrylic tank with two holes at the base was formed and the solution was gradually agitated by hand. Periodically take a 3 mL sample of the mixture and record the UV-Vis absorption spectrum to assess the rate of degradation. The degradation of MB dye based on the exposure to UV light and the effect of Ta-ZnO NWs composite were examined. The maximum peak intensity and position of the MB dye remained at 664 nm, after 105 mins of observation. As time passes, the maximum peak intensity at 664 nm decreases significantly, which is attributed to MB dye degradation, demonstrating that Ta-ZnO NWs composite has strong degradation reactivity against the MB dye (see Figure 6.9 (a, b)). Figure 6.9 (c) depicts a degradation in normalized maximum absorbance as a function of time. According to Figure 6.9 (c), the degradation of MB dye pursues pseudo-first-order kinetics. Slope value Ta-ZnO is higher than ZnO, indicating the higher rate constant. The pH sensors were integrated with the

electronics circuit to perform real-time MB dye degradation illustrated in Figure 6.10. A pH sensor module (Robocraze) and a NodeMCU ESP8266 microcontroller form the basis of this electronic circuit. The pH sensor data from the MB Dye will be streamed to a web server and made available to the public via IoT on their smartphones. A pH sensor uses a potential difference between two electrodes to determine the acidity of water. Small ions enter the borders of the glass membrane when the pH sensor is submerged in an MB dye solution, whereas larger ions remain in the solution. This has the capacity to make a potential difference. The potential difference between electrodes is measured using a pH sensor. It is indeed directly translatable to a pH value. The pH sensor is required to be calibrated in order to obtain accurate results. Standard calibration solutions at pH 4, and pH 7 were used for calibration. The degradation of MB dye by adsorption onto Ta-ZnO composite was found to be slower at first but subsequently became faster as contact duration increased. The degradation of MB dye was found to increase when the pH increased from 6.35 to 6.64 (see Figure 6.10 (a)). Similar literature shows, that increasing trends in the pH value of the MB dye solution in response to UV and solar irradiation were also found (Alkaykh et al., 2020; Khairnar and Shrivastava, 2019).

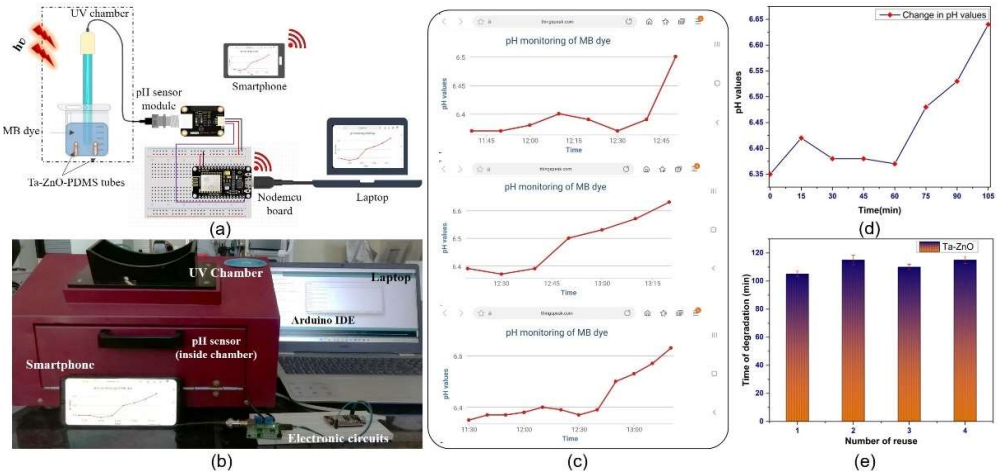


Figure 6.10: (a) Schematic representation of real-time pH monitoring of MB dye degradation using NodeMCU and pH sensor module, (b) pictorial representation of experimental setup, (c-e) Real-time pH values monitored in between experiments at different intervals of time (Total time = 105 min), (f) Real-time change in pH values at an interval of 10 min, and (g) repeatability curve

The degradation characteristics of MB dye molecules on the surface of Ta-ZnO composite are also influenced by the surface charge property of the composite, which is dependent on the pH point of zero charges (pH_{PZC}). The pH_{PZC} of ZnO was 8.5 when determined using the pH drift technique (Khataee et al., 2016). As a result, the surface of the adsorbent is positive at $(pH)_{MB} < (pH_{PZC})$Ta-ZnO, resulting in electrostatic repulsion between MB cations and the Ta-ZnO composite. Furthermore, at a pH of 6.35, H^+ ions are present in high concentrations, competing with dye cations for active sites on Ta-ZnO surfaces, resulting in increased substantial MB degradation on the Ta-ZnO composite surface (Babaei et al., 2016; Senthil Kumar et al., 2014).

Reason for enhanced photocatalytic degradation

UV light (366 nm) is absorbed by ZnO-Ta composites, which allows more electrons to be transferred from lower to higher energy levels. The breakdown of MB in an aqueous solution is mostly caused by hydroxyl radical oxidation. In the presence of dissolved O_2, photoinduced electrons from Ta-ZnO produces O_2^- (superoxide radicals), which can thereafter form H_2O_2 and $\cdot OH$ radicals. Because holes have a high oxidation potential, they can cause H_2O to decompose into extremely reactive $-OH$ groups. Reactive oxygen vacancies that have been cleaved as electron acceptors briefly block photogenerated electrons, inhibit surface recombination of photogenerated electrons and holes, and then attack dissolved O_2. It results in the formation of O_2^- (superoxide radicals) or $-OH$ groups on the surface. The photocatalytic activity of Ta-doped

ZnO may be deduced as follows based on the preceding experimental results. (a) For the breakdown of MB dyes, a Ta-doped ZnO composite coated over a PDMS tube serves as an electron and hole source. In ZnO crystals, Ta^{5+} ions play a crucial role in the creation of hole-electron couples. (b) oxygen and hydrogen-related defects aid in the separation of electron-hole pairs and reduce chemical product combination reactions. (c) In photocatalytic activity, the $-OH$ groups on the surface also serve as an effective center for the mineralization of organic substances. Higher photocatalytic effectiveness is associated with more surface $-OH$ groups.

$$(ZnO - Ta) + h\upsilon \rightarrow (ZnO - Ta)(e^- + h^+) \quad (6.12)$$

$$O_2 + e^- \rightarrow O_2^{\cdot -} \quad (6.13)$$

$$O_2^{\cdot -} + e^- + 2H^+ \rightarrow H_2O_2 \quad (6.14)$$

$$H_2O_2 \rightarrow 2\,(\cdot OH) \quad (6.15)$$

$$h^+ + OH^- \rightarrow \cdot OH \quad (6.16)$$

$$h^+ + H_2O \rightarrow \cdot OH + H^+ \quad (6.17)$$

$$\cdot OH / O_2^{\cdot -} + Dye \rightarrow Degraded_{product} \quad (6.18)$$

The degradation pathway of MB dye can be seen in Figure 6.11. First, the $\cdot OH$ attacked the sulfur-nitrogen conjugated system present in the MB dye molecules, to degrading it into B ((4-(N,N-dimethyl)-aniline) and C(2-amino-4-(N,N-dimethyl)-benzenesulfonic acid). After that, C is degraded to further produce F (2,4-hexadiene-1,6-diol), which cannot be degraded after. The series of reaction causes the other part of C to oxidized to form D (p-nitrobenzene-sulfonic acid), E (benzene-sulfonic acid) (Lin et al., 2018). Similar reaction at B produces I(4-(N,N-dimethyl)-phenol) and J(hydro-quinone), which are then oxidized to G(malonic acid), H(propionic acid), CO_2 and H_2O. These results can be verified by the change in pH values from 6.35 to 6.64.

Recycling test

One of the primary problems for practical applications is the recycling of the produced composite. Ta-ZnO photocatalytic stability for MB degradation was therefore investigated. Five successive cycles of repeatability tests were carried out. The Ta-ZnO were collected after each run, cleaned several times with DI water and ethanol, and dried at 90°C for 18 hours before the next cycle began. The slightly reduced decomposition is due to the intermediate adsorbed on the Ta-ZnO surface and the release of small amounts of Ta-ZnO into the solution during photocatalysis. For Ta-ZnO, cycles 1-4 took 105, 115, 110, and 120 mins respectively. The repeatability of synthesized photocatalyst against the MB dye degradation in shown in Figure 6.10 (e). Table 6.4 presents the comparative assessment of ZnO based composites for photocatalytic degradation.

Table 6.4: Previous work on the degradation of MB dye

Photocatalyst	Exposing source	Irradiation time	Dye	Ref
CA–CNT/TiO_2–NH_2	UV light	300 min	MB	(Salama et al., 2018)
WO_3 nanoplate	UV light	105 min	MB	(Gupta et al., 2020)
BiOI coating	UV light	150 min	MB	(Hao et al., 2020)
rGO/$CaSnO_3$ nanocomposite	UV light	150 min	MB	(Venkatesh et al., 2020)

Ta-ZnO-PDMS	UV light	105 min	MB	Present work

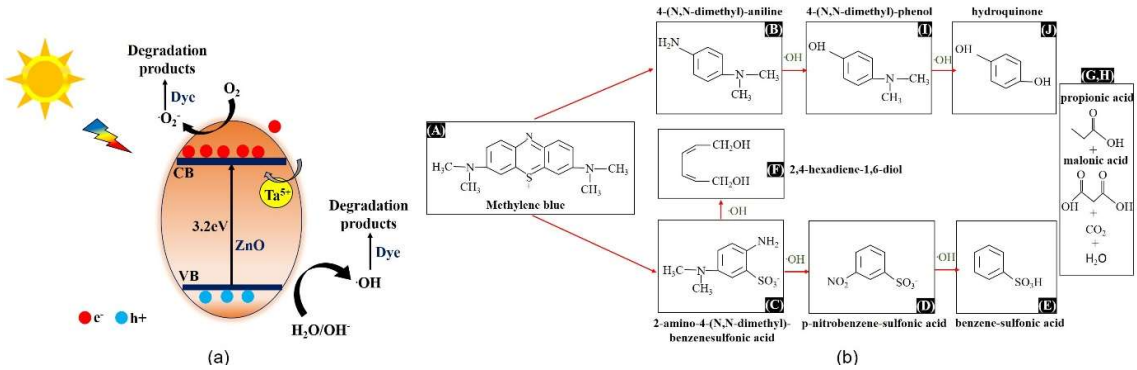


Figure 6.11: (a-b) Possible degradation mechanisms of MB dye using Ta-ZnO composite

6.2.4 Summary

In this work, we present a potential approach for fabricating a bioinspired tube using a non-toxic, biocompatible, and lotus-like microstructure replicated on PDMS materials coated with Ta-ZnO composite, which will undoubtedly provide a greater number of active sites for various applications. A real-time MB dye degradation is also monitored using the IoT technique by integrating a NodeMCU microcontroller board as a control center and a pH sensor as a tool for detecting the change in pH value of the MB dye. These lotus-like microstructure replicated on PDMS tubes were responsible for delivering a high surface-to-volume ratio for the formation of Ta-ZnO composite, as confirmed by SEM and EDS results. Further, this superhydrophobic (CA:168.0°) bio-inspired polymeric platform was modified by optimizing the surface roughness and coating it with low-surface-energy Ta-ZnO NWs composites, paving the way for its to be utilized in "self-cleaning" water treatment facilities. The photocatalytic reaction of the Ta-ZnO NWs composite coated PDMS tube took 105 mins, which is faster than ZnO. These photocatalysts lead to "waste control using Ta-ZnO NWs composites," which opens up new possibilities for flexible and biocompatible environmental remediation platforms. Furthermore, this study might well assist researchers in better understanding the relationship between both synthesized composite structures and their photocatalytic degradation.

...